Nuclear Science and Techniques (2025) 36:17
https://doi.org/10.1007/s41365-024-01614-y

Precision storage lifetime measurements of highly charged heavy ions in the CSRe storage ring using a Schottky resonator

Qian Wang[1] · Xin-Liang Yan[1,2] · Guang-Yu Zhu[1] · Shahab Sanjari[3,4] · Li-Jun Mao[1,2] · He Zhao[1,2] · Yuri A. Litvinov[3] · Rui-Jiu Chen[3] · Meng Wang[1,2] · Yu-Hu Zhang[1,2] · You-Jin Yuan[1,2] · Jun-Xia Wu[1,2] · Hong-Yang Jiao[1,2] · Yue Yu[1,2] · Zu-Yi Chen[1,2] · Yin-Fang Luo[1,2]

Received: 11 September 2024 / Revised: 10 October 2024 / Accepted: 21 October 2024 / Published online: 22 December 2024

Abstract
Schottky mass spectrometry utilizing heavy-ion storage rings is a powerful technique for the precise mass and decay half-life measurements of highly charged ions. Owing to the nondestructive ion detection features of Schottky noise detectors, the number of stored ions in the ring is determined by the peak area in the measured revolution frequency spectrum. Because of their intrinsic amplitude-frequency characteristic (AFC), Schottky detector systems exhibit varying sensitivities at different frequencies. Using low-energy electron-cooled stored ions, a new method is developed to calibrate the AFC curve of the Schottky detector system of the Experimental Cooler Storage Ring (CSRe) storage ring located in Lanzhou, China. Using the amplitude-calibrated frequency spectrum, a notable refinement was observed in the precision of both the peak position and peak area. As a result, the storage lifetimes of the electron-cooled fully ionized $^{56}Fe^{26+}$ ions were determined with high precision at beam energies of 13.7 and 116.4 MeV/u, despite of frequency drifts during the experiment. When electron cooling was turned off, the effective vacuum condition experienced by the 116.4 MeV/u $^{56}Fe^{26+}$ ions was determined using amplitude-calibrated spectra, revealing a value of 2×10^{-10} mbar, which is consistent with vacuum gauge readings along the CSRe ring. The method reported herein will be adapted for the next-generation storage ring of the HIAF facility under construction in Huizhou, China. It can also be adapted to other storage ring facilities worldwide to improve precision and enhance lifetime measurements using many ions in the ring.

Keywords Lifetime measurement · Schottky mass spectrometry · Sensitivity response · Highly charged heavy ion · Resonator · UH vacuum · Nondestructive diagnostics

1 Introduction

Mass and lifetime are the basic properties of atomic nuclei. To date, approximately 3400 nuclides have been identified, of which fewer than 300 are stable nuclei concerning radioactive decay [1]. Theoretical predictions indicate the existence of numerous additional particle-bound nuclei [2, 3]. The discovery of new isotopes and measurements of their mass and decay characteristics require powerful radioactive ion beam facilities and fast, sensitive detection techniques [4]. Utilizing heavy-ion storage rings coupled to radioactive beam lines, time-resolved Schottky mass spectrometry has been proven to be a powerful tool for measuring the radioactive decay of highly charged ions and investigating exotic decay modes [5–8]. Schottky mass spectrometry is based on nondestructive Schottky detectors mounted on storage rings. Currently, only three operational heavy-ion storage ring facilities exist worldwide: the GSI-ESR (Germany) [9], HIRFL-CSRe (China) [10], and RIKEN-R3 (Japan) [11]. Schottky mass spectrometry was implemented at all three facilities [12–14] and is planned for future storage ring facilities under construction: the SRing in Huizhou, China [15] and CR-ring in Darmstadt, Germany [16].

This work was supported by the National Key R&D Program of China (No. 2023YFA1606401 and 2018YFA0404401), the Young Scholar of Regional Development, CAS ([2023] 15), Chinese Academy of Sciences Stable Support for Young Teams in Basic Research (No. YSBR-002), and Special Fund for Strategic Pilot Technology of Chinese Academy of Sciences (No. XDB34000000).

Extended author information available on the last page of the article

The experimental Cooler Storage Ring (CSRe) was commissioned at the Heavy Ion Research Facility in Lanzhou in 2007 [17]. Since its inception, it has been dedicated to advancing the field of isochronous mass measurements by utilizing time-of-flight (TOF) detectors [18, 19]. Owing to the destructive detection mechanism of TOF detectors, the beam lifetime is significantly reduced. Consequently, lifetime measurements using TOF detectors have been limited to the range of several tens to hundreds of microseconds, and one experiment has been conducted for $^{94m}Ru^{44+}$ [20]. For CSRe Schottky mass spectrometry, two parallel metal-plate Schottky detectors were installed in the CSRe [21]. In 2011, these were replaced by a pillbox resonator-cavity Schottky detector [22], similar to that used in ESR [23], to improve the sensitivity of the CSRe Schottky mass spectrometer [24]. In 2014, the first decay-lifetime measurements of radioactive fully ionized ions, $^{49}Cr^{24+}$ and $^{53}Fe^{26+}$, which were produced by the projectile fragmentation of the ^{58}Ni beam, were performed using the CSRe Schottky resonator [25]. Subsequently, the data acquisition system of the Schottky detector was upgraded to enable long-term continuous data recording [26]. During this period, three test experiments of beam lifetime measurements were conducted at the CSRe using ^{58}Ni, ^{78}Kr, and ^{36}Ar beams. In 2020, a versatile baseline-correction method called BrPLS was developed to subtract the background from the signal peaks in measured Schottky spectra [27]. The results showed that the unstable experimental conditions, such as drifts in the ion revolution frequency and broadening of the frequency distribution caused by a wide momentum distribution, unstable magnetic fields [28], or unstable electron cooler voltages, have hindered precise beam lifetime measurements.

Owing to the nondestructive detection feature of Schottky noise detectors, heavy ions can be measured without disturbing the storage rings [29]. The stored ion species are distinguished by their revolution frequencies, which correspond to their mass-to-charge ratios. This is the foundational principle of storage ring mass spectrometry. The high mass-resolving power of the storage ring can be enhanced using an electron cooling device and/or a ring with a specially designed isochronous ion optical configuration [25, 30–34], which is crucial when the nuclei of interest are among a vast number of other ion species stored in the ring simultaneously. Frequency spectra were measured continuously to obtain lifetime measurements using time-resolved Schottky mass spectrometry. The peak area of the revolution frequency in the spectra was proportional to the signal power induced by the corresponding ions in the Schottky detector [22]. By observing the reduction in the peak area, the decline in ion numbers as a function of storage time can be monitored, and the decay half-life can be deduced [6].

Traditionally, parallel-plate-type capacitive Schottky detectors have been used to detect electromagnetic signals induced by passing ions [35, 36]. Higher sensitivity can be achieved using a resonant cavity [37]. The main advantage of using resonant cavities as Schottky pickups is their increased sensitivity to the characteristic resonance frequency of the cavity; thus, a higher signal-to-noise ratio can be achieved [14, 22, 23]. Moreover, the higher resolution obtained at higher frequencies provides an added benefit [38]. These enhancements make them suitable devices for the fast detection of low-yield exotic isotopes, even for single ions. For example, this detector was used to directly monitor the decay from parent to daughter nuclei in single-ion decay measurements [39].

Individual ion counting is not possible in many-ion decay half-life measurement experiments (see review article [40] and references therein). Therefore, the calibration of the peak area is necessary before the corresponding particle count can be accurately determined. This calibration involves understanding the sensitivity of a Schottky detector system, which varies with frequency and can be characterized by an amplitude-frequency characteristic (AFC) curve. Compared with parallel-plate detectors, the cavity-resonator detector has an enhanced signal from ions and an elevated background-noise level near the resonance frequency. This increased sensitivity results in a more pronounced sensitivity change across the same frequency range.

Typically, an electron cooling device is used in a storage ring to stabilize the frequency of heavy ions [41–44]. However, the interaction between the stored ions and electron beam from the electron cooling device introduces additional ion beam loss, which alters the decay constant of the ions in the storage ring [45]. When electron cooling is absent or deactivated, the signal peak of a particular ion species broadens over a wide revolution frequency range because of the large momentum spread, and shifts owing to the ongoing energy loss from collisions with the residual gas in the vacuum pipe [25]. Thus, the amplitude-frequency variation of the detector system can distort the ion peak shapes, leading to peak areas that do not directly correspond to the actual number of ions present.

In this study, a new method is developed to calibrate the AFC curve (sensitivity curve) of the Schottky detector system installed in the CSRe storage ring. This method, combined with the background-noise subtraction technique developed in our previous study [27], has enabled the precise determination of the storage lifetime of stable $^{56}Fe^{26+}$ ions in the ring, despite the broad frequency spread and unexpected frequency drifts. Once the revolution frequency spectra are normalized to the AFC curve, we can restore the peak shape and determine the peak center with better precision. This method improves the precision and enhances the capability of beam lifetime measurements using many ions in the ring and is complementary to single-ion decay measurements [39]. When the electron cooling system is turned off,

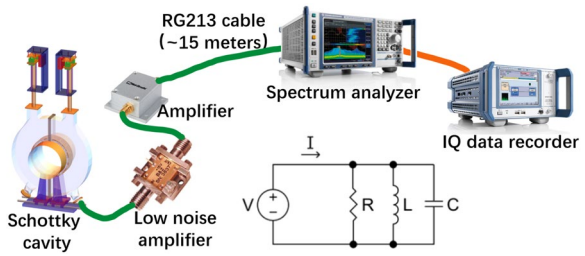

Fig. 1 (Color online) Schematic illustration of the resonator Schottky detector system and its corresponding equivalent RLC circuit [22]. The ion signal is captured by the Schottky cavity, amplified by a low-noise amplifier, filtered by a band-pass filter, and further amplified before being transmitted to the frequency analyzer via a 15-m coaxial cable. The signal is then digitized by the spectrum analyzer and stored by the IQ data recorder

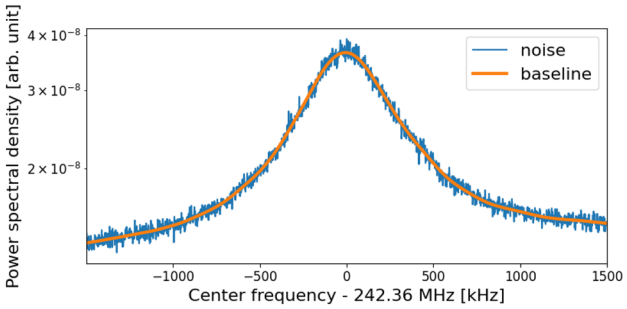

Fig. 2 Blue histogram: the measured thermal noise in the frequency domain when no beam is present in the CSRe. It can be used as a reference baseline in the subsequent measurement to extract the signal power induced by the storied ions. Orange line: the estimated baseline determined using the method of [27]. The reference level is set to -50 dBm, data acquisition time is 852.5 ms, frequency resolution is 0.92 kHz, and DAQ sampling rate is 3.75 MSamples/s

the ion beam gradually loses energy. By tracking the rate of change in the central frequency of the beam, we determine the effective vacuum level experienced by the ions stored in the storage ring. The methodology developed in this study will be adapted for the future SRing facility in Huizhou, China. It can also be adapted by other heavy-ion storage ring facilities to improve precision and enhance the capability of beam lifetime measurements using many ions.

2 Time-resolved Schottky mass spectrometry at heavy-ion storage ring

A schematic of the Schottky detection system at the CSRe facility is shown in Fig. 1. As the ions pass through the cavity, they induce image charges and deposit energy, creating Schottky noise. This noise was extracted from the cavity using magnetic couplers [23], amplified using a low-noise amplifier, and finally recorded using a spectrum analyzer. The measured data were analyzed online or offline revealing peaks at the ion revolution frequency at each harmonic in the frequency domain (hereafter referred to as the frequency spectrum), obtained using Fourier transformation.

2.1 Reference baseline in the measured frequency spectrum

Within the bandwidth of the detection system, the measured noise power includes both the signal power $P_{\mathrm{ion}}(f)$ from the circulating ions in the ring and the thermal noise power $P_{\mathrm{thermal}}(f)$ of the detection system:

$$P_{\mathrm{total}}(f) = P_{\mathrm{thermal}}(f) + P_{\mathrm{ion}}(f). \tag{1}$$

Owing to the resonant nature of the cavity, the thermal noise exhibits a Lorentzian-like distribution in the frequency domain. Experimentally, the power density profile of the thermal noise in the frequency domain can be measured when the beam is off [27]. The result of the averaged spectrum can serve as a benchmark for the reference baseline (blue histogram in Fig. 2) and is subtracted from the frequency spectrum measured when the beam is present. Alternatively, the baseline can be estimated using the method described in Ref. [27] (orange line shown in Figs. 2 and 3). The advantage of this method is that baseline measurements can be performed *in situ* when the beam is present, and a smooth reference baseline can be obtained.

2.2 Information on the stored ions extracted from frequency peaks

After subtracting the thermal noise baseline, the remaining spectral components in the frequency spectrum are attributed to the periodic motion of the ions. Throughout this study, we consider only the case of a coasting (i.e., not bunched) ion beam [46, 47].

The Schottky noise originating from individual ions circulating in the ring at a specific revolution frequency f_{rev} manifests as a series of distinct peaks in the frequency spectrum, each corresponding to a different harmonic number, $h = 1, 2, 3, \ldots$. The power density of each harmonic can be expressed as [6]

$$\frac{\mathrm{d}P_{\mathrm{ion}}(f)}{\mathrm{d}f} = 2q^2e^2 \sum_{h=1}^{+\infty} \frac{f^2}{h^3} |H(f)|^2 \xi(f), \tag{2}$$

where $|H(f)|$ represents the AFC function of the Schottky detector system, $\xi(f)$ is the normalized revolution frequency distribution of the ions, and q is their electric charge. When h is the harmonic number, the integration of the power density spectrum near a certain harmonic frequency hf_{rev} results in

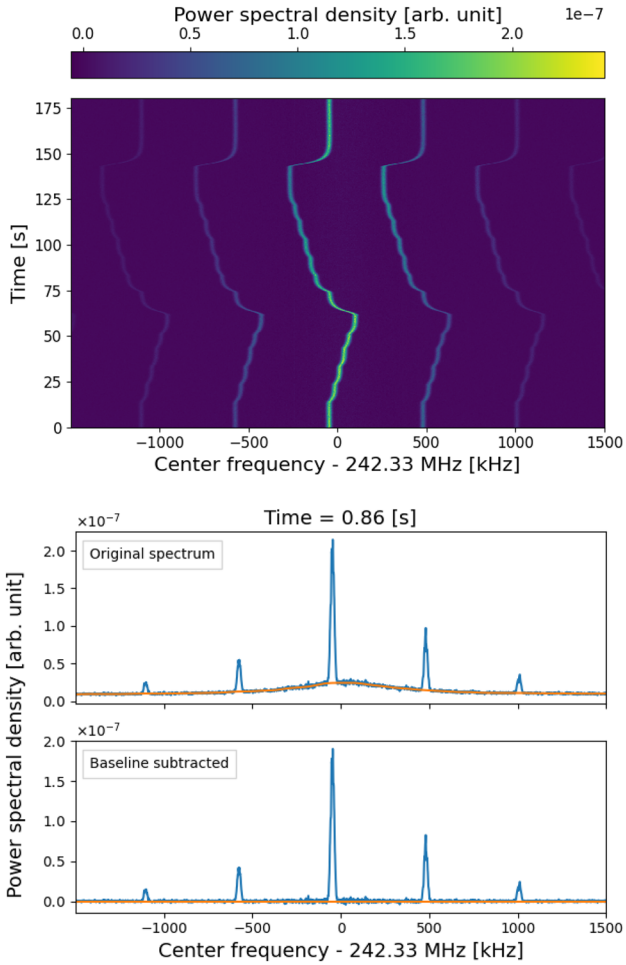

Fig. 3 (Color online) Top panel: Time-resolved Schottky spectrum of electron-cooled $^{56}Fe^{26+}$ beam with energy of 13.6 MeV/u. The velocity of the ions was shifted in steps such that the revolution frequency change covers the entire measurement-frequency range of 3 MHz. The time resolution is 86 ms/channel, and the frequency resolution is 0.92 kHz/channel. Middle panel: Single frame from the top panel at time = 0.86 s, including 5 harmonics $h = 614, 615, \ldots, 618$. The blue line indicates the original power density of the spectrum. The orange line is the estimated baseline [27]. Bottom panel: The same spectrum as the middle frame after the baseline was subtracted

$$P_{\text{ion}} = \int_{hf_{\text{rev}}-\delta}^{hf_{\text{rev}}+\delta} \frac{\mathrm{d}P_{\text{ion}}}{\mathrm{d}f}\mathrm{d}f = 2N\left[|H(hf_{\text{rev}})|qef_{\text{rev}}\right]^2, \tag{3}$$

where N is the number of ions of a specific ion species. The value of δ is typically set to five standard deviations of the corresponding frequency peak hf_{rev}. The second equality in Eq. (3) holds true on the condition that the frequency spread of each ion remains sufficiently small during the measurement period. For single-ion decay-measurement experiments in heavy-ion storage rings, the decay event is unambiguously determined by the disappearance of the parent ion and appearance of the daughter ion [39]. In other cases, the fluctuation in the ion number can be monitored by measuring the peak area in the frequency spectrum associated with the ion species of interest and monitoring its evolution as a function of time. To achieve this, the calibration of the AFC function of the detection system is important. Determination of the AFC function relies on the fact that the measured signal peak areas that correspond to the same stored ion species in the ring remain consistent at any revolution frequency harmonic hf_{rev} [46].

3 Calibration of the AFC function

The resonant Schottky cavity detector installed in the CSRe has a pillbox design, as shown in Fig. 1. Owing to the characteristics of the equivalent RLC circuit, an AFC form similar to that of the cavity [22, 23, 48, 49] was used for modeling the AFC function of the entire detector system:

$$|H(f)| = \frac{R_{\text{sys}}\gamma\sqrt{\zeta}}{\sqrt{1 + Q_{\text{sys}}^2\left(\frac{f}{f_{\text{sys}}} - \frac{f_{\text{sys}}}{f}\right)^2}}, \tag{4}$$

where R_{sys} is the resistance of the equivalent RLC circuit of the entire system, ζ is the loss factor quantifying the energy loss to the wake fields [50], and γ is the relativistic Lorentz factor of the ions. In addition, Q_{sys} and f_{sys} are the effective quality factor and resonant frequency of the system, respectively. The AFC curve of the Schottky cavity was measured offline using a network analyzer. In contrast, determining the AFC curve for the entire detection system requires online beam experiments. The resulting AFC curve is influenced not only by the AFCs of the cavity, electronic components, and cables, but also by the AFC of the spectrum analyzer. The AFC of the system can be determined by leveraging the features of multiple peaks of the same ion species that appear simultaneously at several frequency harmonics. If we can simultaneously measure at least two frequency harmonics of the same ion species in the spectrum, we can determine the relative sensitivity ratio between the two harmonic frequencies within the same spectrum.

The optimal method for measuring the AFC curve employs electron-cooled low-energy beams. Low ion energy leads to small frequency intervals between adjacent harmonics. Electron cooling is essential to ensure that the ion peak is sufficiently narrow such that the corresponding AFC region under it can be considered constant. Consequently, multiple revolution frequency harmonics can be detected simultaneously within the frequency range of the data acquisition (DAQ) system. By adjusting the electron cooler voltage, we can shift the center frequencies in steps to collect more data points along the AFC curve, thereby enabling

the determination of the entire curve within the measured frequency range.

3.1 Calibration measurement

In the experiment, the electron-cooled $^{56}Fe^{26+}$ ions at an energy of 13.6 MeV/u were utilized to measure the AFC curve within the 3-MHz bandwidth around the resonant frequency of the Schottky detector system. The measured time-resolved frequency spectrum is presented in Fig. 3. Up to six harmonics of the revolution frequency were simultaneously covered. By adjusting the voltage of the electron cooler from 126.6 kV to 129.8 kV, the velocity of the ions was altered in 13 increments [51, 52]. Consequently, the center frequency of each harmonic was shifted by approximately 600 kHz.

As the number of stored ions decreases because of inevitable particle losses as $N = N_0 e^{-\lambda_t t}$, the integrated power decreases as a function of time:

$$P(t) = P_0 e^{-\lambda_t t}, \tag{5}$$

where λ_t is the decay constant, $P_0 = 2N_0\left[|H(hf_{\mathrm{rev}})|qef_{\mathrm{rev}}\right]^2$, and N_0 is the initial number of ions. The storage lifetime τ of the ions can be obtained from the decay constant using $\tau = 1/\lambda$. Based on Eq. (3)–(5), the integrated power of the ion beam at each harmonic in the spectrum can be expressed as a function of the center frequency of the harmonic $f = hf_{\mathrm{rev}}$ and time t, denoted as

$$P(f,t|A_0,\lambda_t,Q_{\mathrm{sys}},f_{\mathrm{sys}}) = \frac{A_0}{1+Q_{\mathrm{sys}}^2\left(\frac{f}{f_{\mathrm{sys}}}-\frac{f_{\mathrm{sys}}}{f}\right)^2}e^{-\lambda_t t}, \tag{6}$$

where $A_0 = 2N_0\zeta\left(R_{\mathrm{sys}}\gamma qef_{\mathrm{rev}}\right)^2$ denotes the initial peak area. Parameters A_0 and λ_t are related to the properties of the ion beam, whereas Q_{sys} and f_{sys} are uniquely associated with the attributes of the detector system.

The specific data processing steps are as follows:

1. The reference baseline is estimated and subtracted to generate the background-free spectrum using the method described in Ref. [27]. See Fig. 3.
2. For each spectrum at time t_j ($j = 1, 2, \ldots, n$), the peak area is calculated by simple integration for each peak at different harmonics. Here, n is the number of bins in time during the continued spectrum-recording process. This yields the experimental value $P_{i,j}^{\mathrm{exp}}$ at frequency $f = f_i$ ($i = 1, \ldots, 6$ harmonic) and time $t = t_j$, see Fig. 4.
3. Data segmentation. Refer to the next subsection for more details.
4. The function $P(f,t|A_0,\lambda_t,Q_{\mathrm{sys}},f_{\mathrm{sys}})$ based on Eq. (6) is fitted to the experimental value $P_{i,j}^{\mathrm{exp}}$ to obtain the parameters A_0, λ_t, Q_{sys}, and f_{sys}.

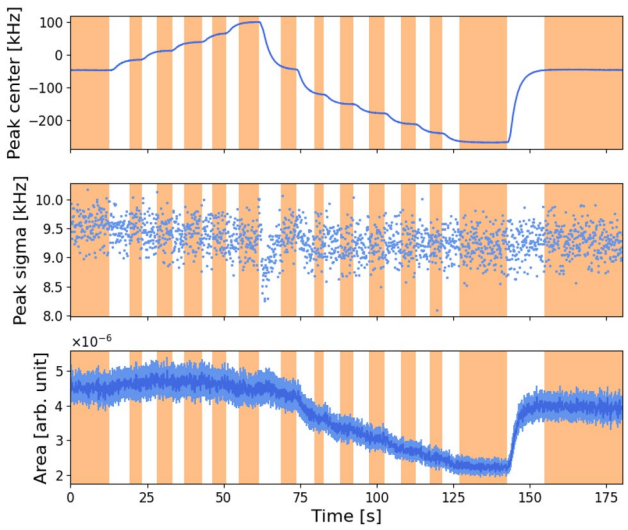

Fig. 4 (Color online) Time evolution of the peak of $^{56}Fe^{26+}$ ions near 242.33 MHz (harmonic number $h = 616$): center frequency (top), peak width (middle), and peak area (bottom). At approximately 63 s, when the center frequency of the harmonic changes abruptly, the peak width is also affected. Therefore, we only utilized the 14 data segments when the center frequency was stable, as indicated by the orange regions

5. The values of Q_{sys} and f_{sys} are implemented into Eq. (4) to obtain the AFC curve of the detection system. These two parameters are independent of the ion beam and can be used throughout the experiment if the detector settings were fixed.

3.2 Error estimation of Q_{sys} and f_{sys}

The function $P(f,t|A_0,\lambda_t,Q_{\mathrm{sys}},f_{\mathrm{sys}})$ in Eq. (5) is a bivariate nonlinear function. In the fitting procedure, the task is to determine the optimized combination of parameters that minimizes the following objective function:

$$S = \sum_j \sum_i \left(P_{i,j}^{\mathrm{exp}} - A_0 e^{-\lambda_t t_j}\left(1+Q_{\mathrm{sys}}^2\left(\frac{f_i}{f_{\mathrm{sys}}}-\frac{f_{\mathrm{sys}}}{f_i}\right)^2\right)^{-1}\right)^2. \tag{7}$$

Although the processing steps are straightforward, numerous challenges exist. These include:

a. Data segmentation. A_0 in Eq. (7) must be accurately determined. During the measurement, we adjusted the electron cooling 13 times. Figure 4 illustrates the changes in the center frequency, width, and area (i.e., average ion power) of the ion peaks of the 616th harmonic. Upon completion of the electron cooling adjustment, the center frequency and peak width fluctuate significantly. Within a few seconds, the velocity of the

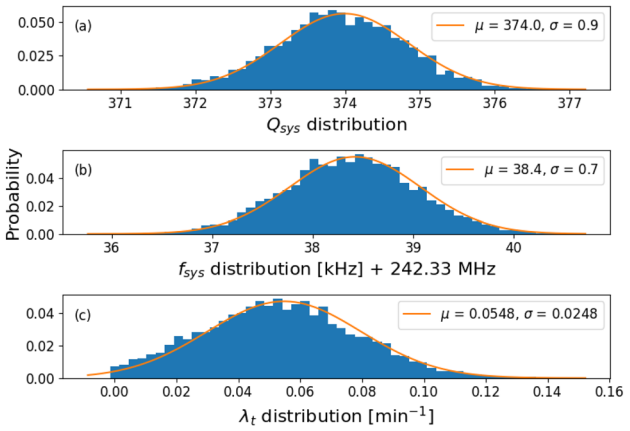

Fig. 5 Parameter distributions obtained by Monte Carlo calculations: the probability distributions of parameters **a** Q_{sys}, **b** f_{sys}, and **c** λ_t. The mean and variance of all the parameters are calculated using the Gaussian distribution with mean value μ and sigma value σ

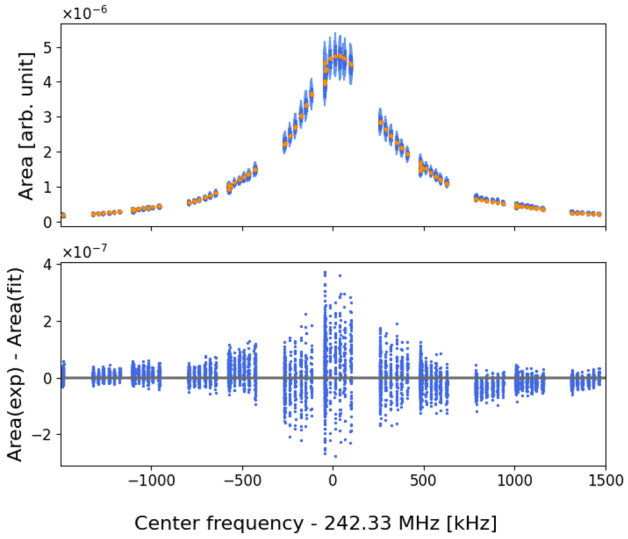

Fig. 6 Top panel: comparison between the measured (blue dots) and calculated peak areas (orange dots) using fitted AFC function of the CSRe Schottky detector system. A sudden decrease in the data points is observed owing to the frequency range being passed through twice during the measurements, as shown in Fig. 3. Bottom panel: differences between the measured and fitted peak area

ions reach equilibrium, and the peak position stabilizes. Consequently, the data are filtered into 14 segments, indicated by the orange regions in Fig. 4, where the equilibrium was reached. Instead of using a single initial peak area parameter A_0, fourteen independent initial peak areas $A_{0,k}(k = 1, 2, \ldots, 14)$ are assigned to the corresponding data segments. The timing t_j in each data segment is also readjusted accordingly to the new starting points so that $A_{0,k}$ is encountered at $t_{k,j} = 0$. Hence, the objective function of the fitting is altered to:

$$S = \sum_{k=1}^{14} \sum_{j=1}^{n_k} \sum_{i=1}^{N_k} \left(P_{k,j,i}^{\exp} - A_{0,k} e^{-\lambda_t t_{k,j}} \left(1 + Q_{\text{sys}}^2 \left(\frac{f_{k,i}}{f_{\text{sys}}} - \frac{f_{\text{sys}}}{f_{k,i}} \right)^2 \right)^{-1} \right)^2, \tag{8}$$

where N_k represents the number of measured harmonics in the spectrum of each data segment.

b. Monte Carlo calculations are used to estimate the value and error of the fitting parameters: Q_{sys}, f_{sys}, λ_t, and $A_{0,k}(k = 1, 2, \ldots, 14)$. Part of the results is shown in Fig. 5. The estimated value and error of each parameter are the mean and variance of its distribution, respectively.

3.3 Fitting results of the AFC function

The characteristic parameter values of the AFC of the CSRe Schottky system were determined to be $Q_{\text{sys}} = 374.0 \pm 0.9$ and the resonant frequency $f_{\text{sys}} = 242.3684 \pm 0.0007$ MHz, as illustrated in Fig. 5. The resulting peak areas calculated using the obtained AFC parameters are shown as orange dots in Fig. 6. The fitting residuals are uniformly distributed around zero, indicating a good estimation of Q_{sys} and f_{sys}. Notably, owing to the larger error in the peak area determinations, a wider spreading of the residuals is evident at frequencies close to the resonance, near 242.36 MHz.

The measured Q value of the detection system is smaller than that of the Schottky cavity, $Q_{\text{cavity}} = 496.8$ [22]. This is reasonable because other components of the system can deteriorate the resonance sensitivities. To achieve a higher Q_{sys}, and thus, a higher sensitivity of the heavy-ion detection, new Schottky resonant cavities without ceramic beam pipes are under construction for next-generation SRing facilities [15]. Thus, a Q_{cavity} four times higher can be reached with a stainless steel cavity and 20 times higher with a copper-coated cavity.

4 Application of the AFC function to the storage lifetime measurement of $^{56}Fe^{26+}$ ions at different energies

After the AFC curve of the Schottky detector system was determined, we measured the storage lifetime of the fully ionized $^{56}Fe^{26+}$ ions under the same detector settings. The decay constant λ of the ions was determined from the normalized peak area in the revolution frequency spectrum, and the storage lifetime was converted from the decay constant by $\tau = 1/\lambda$. The results are summarized in Table 1.

Two beam energy settings were used, and the electron cooling only had an ON or OFF status. No voltage or current adjustments were made during the ON state, which was different from the measurement procedure used for AFC

Table 1 Measured decay constant λ(Exp) of the $^{56}Fe^{26+}$ ions in the CSRe operated under the internal target mode ($\gamma_t = 2.457$) [10]. The storage lifetime can be calculated by $\tau = 1/\lambda$. The theoretical decay constants λ(Theory) were also listed [53–59], where realistic parameters of the CSRe cooler (electron-beam temperature of 0.5 eV, current of 0.2 A, radius of 4 cm) and vacuum (2×10^{-10} mbar, 20 °C) were utilized in the computation. For ions with energies of 13.7 MeV/u, no suitable theoretical formula estimated their lifetime, and only the upper and lower bounds of the lifetime were given based on References [53, 59]

ECooler status	Energy (MeV/u)	γ	λ(Exp) (min^{-1})	λ(Theory) (min^{-1})
ON	116.4	1.125	0.00685(9)	0.00648
OFF	116.4	1.125	0.00051(4)	0.0003
ON	13.7	1.027	0.0476(1)	0.03066< λ_s <0.6968
OFF	13.7	1.027	0.035(2)	0.0178< λ_s <0.684

determination. The first energy was set to 13.7 MeV/u, which was the same as the setting for the AFC curve measurement. The measured decay constant of the electron-cooled $^{56}Fe^{26+}$ ions was 0.0476(1) min^{-1}, which was consistent with $\lambda_t = 0.054(25)$ min^{-1} determined during the AFC determination measurement (see Fig. 5c). Table 1 shows that the decay constant of the fully ionized $^{56}Fe^{26+}$ is smaller when electron cooling is switched off. This is because the electron beam of the cooler introduces an additional beam loss mechanism to the stored ion beam.

When the electron cooler was ON, the decay constants of the stored $^{56}Fe^{26+}$ ions at the higher beam energy of 116.4 MeV/u were more than one order of magnitude smaller than those at 13.7 MeV/u. After electron cooling was switched off, the decay constant decreased by another order of magnitude at 116.4 MeV/u. This indicates that at this beam energy, the main contribution to ion loss is from the electron cooling process. Assuming realistic parameters of the CSRe cooler, an electron-beam vertical temperature of 0.5 eV, electron current of 0.2 A, electron-beam radius of ~ 4 cm, vacuum of $\sim 2 \times 10^{-10}$ mbar (see Sect. 4.2), and room temperature of 20 °C inside the vacuum pipe, the calculated theoretical decay constants agree well with the measured values, both at high energy [53–58] and low beam energy [53, 58, 59], as shown in the last two columns of Table 1.

The importance of applying the AFC curve in lifetime measurements is clearly demonstrated by the set of measurements with a beam energy of 116.4 MeV/u. The subsequent sections utilize the findings from this beam setting to elucidate the indispensability of the AFC curve for many-ion storage lifetime measurements in the ring.

4.1 Correcting for sudden peak area changes

Figure 7 illustrates the Schottky spectrum of the electron-cooled $^{56}Fe^{26+}$ ion beam at 116.4 MeV/u. The center frequency of the peak unintentionally underwent five abrupt shifts, as shown in Fig. 7b. In the original spectra, before applying AFC normalization, this directly resulted in the corresponding rapid change and restoration of both the peak center frequency and peak area within 2 min, as depicted

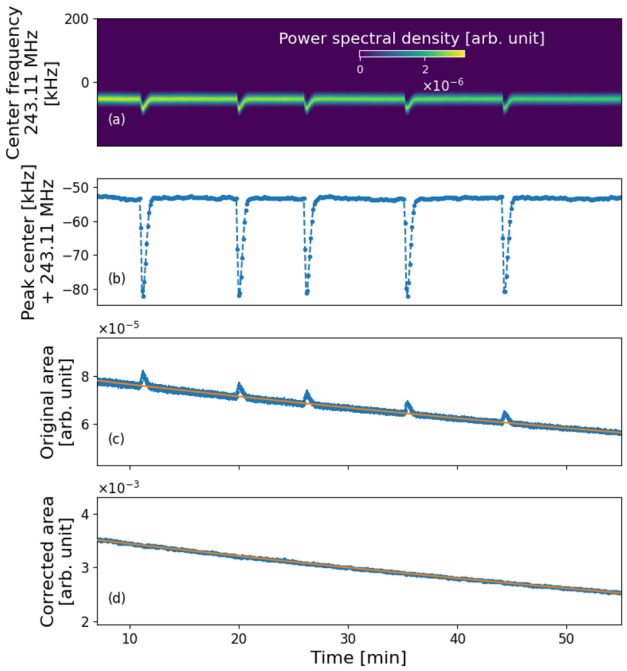

Fig. 7 (Color online) **a** Time-resolved Schottky spectrum of $^{56}Fe^{26+}$ at beam energy of 116 MeV/u with electron cooling switched on. The horizontal axis is the observation time, the vertical axis represents frequency, and the power density is represented by color. The frequency resolution is 0.12 kHz/channel, and the time resolution is 6.39 s/bin. The evolutions of the **b** peak center frequency and peak area **c** before and **d** after AFC normalization as a function of time are also shown. Five jumps are clearly observed during the acquisition period

in Fig. 7b, c. Considering the data affected by these five perturbations, the ion storage lifetime was determined to be $\tau = 144(8)$ min by using the entire dataset. Excluding the peak area affected by the five perturbations, we deduced $\tau = 145(2)$ min with the reduced dataset. After the AFC curve was used to normalize the ion peak areas, as shown in Fig. 7d, the effects of perturbations were mitigated. The normalized peak area followed an exponential decay trend despite frequency shifts. This indicated that the swift frequency shifts did not introduce an additional loss of ions during the experiment. The ion storage lifetime derived

from the normalized peak area was 145(2) min. This result was consistent with that obtained using the reduced dataset. The accuracy was enhanced by 4%, not only because of the increased statistics in comparison with those derived from the reduced dataset, but also because of the accurate determination of the peak area utilizing the AFC normalization process. The five observed perturbations can be attributed to the sudden charging and discharging of the high-voltage power supply of the electron cooler. In the case of similar frequency drifts, the AFC curve serves as a key for correctly and precisely determining the storage lifetime of the stored ions.

4.2 Effective vacuum experienced by the stored ions

After the electron cooling is turned off, the energy loss of the beam caused by collisions between ions and the residual gas can no longer be compensated for. Consequently, the momentum of the beam ions decreases, and the momentum spread increases gradually. The absolute rate of frequency change $\mathrm{d}f/\mathrm{d}t$ is proportional to the effective vacuum experienced by the stored ions. Using the AFC-normalized spectrum, the peak shape can be restored, and the peak center frequency can be determined with better precision. The effective vacuum can be derived from the obtained $\mathrm{d}f/\mathrm{d}t$, and the storage lifetime of the ion can be obtained from the normalized peak area, which decreases as a function of storage time.

As shown in Fig. 8, upon deactivating the electron cooling (at approximately 0.8 s), the ion momentum spread began to increase and the center frequency of the ion peak drifted toward lower frequencies. Based on the measured AFC curve in Fig. 6, the frequency drifts toward the region where the maximum AFC of the system is situated. This is why the peak area, which is deduced from the spectra before AFC normalization, increases over time, as shown in Fig. 8c. In contrast, the decreasing trend was restored, and the storage lifetime was determined to be 1954(139) min from the normalized peak area using the AFC curve of the detector system, as shown in Fig. 8d.

Based on the rate of the peak center frequency change observed in Fig. 8b, $\mathrm{d}f/\mathrm{d}t \approx 23$ Hz/s, the ion energy loss rate $\mathrm{d}E/\mathrm{d}t$ can be deduced using $\mathrm{d}f/f = (\gamma^{-2} - \gamma_\mathrm{t}^{-2})\mathrm{d}E/E$, where $\gamma_\mathrm{t} = 2.457$ and γ is the Lorentz factor of the ions. This calculation yields a value of $\mathrm{d}E/\mathrm{d}t \approx 1.89$ keV/s. Assuming a room temperature of 20°C and a measured composition of the residual gas (90% H_2, 5% CO, and 5% N_2) inside the vacuum pipe [60], the equivalent vacuum inside the CSRe beam pipe can be estimated using the Lise++ program [61] by considering the energy loss of ions through the material. This was determined to be approximately 2×10^{-10} mbar. This value represents the effective vacuum experienced by

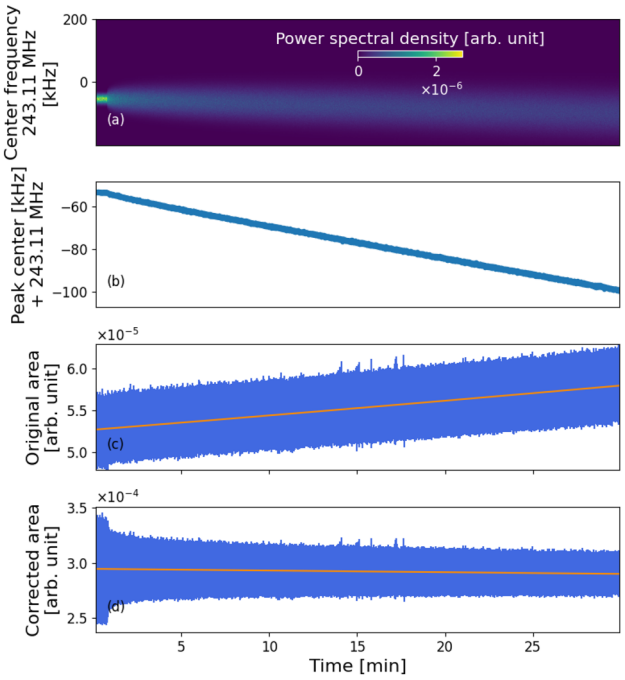

Fig. 8 (Color online) **a** Time-resolved Schottky spectrum of $^{56}Fe^{26+}$ at beam energy of 116 MeV/u. Electron cooling is switched off at approximately 0.8 s. The evolutions of the **b** peak center frequency and peak area **c** before and **d** after AFC normalization as a function of time are also shown. After the electron cooler was switched off, the frequency spread increased and the center frequency gradually drifted toward lower frequencies. The frequency resolution is 0.24 kHz/channel, and the time resolution is 0.32 s/bin

stored $^{56}Fe^{26+}$ ions. In total, 11 ultrahigh vacuum gauges were used in the experiment and were distributed evenly along the CSRe ring. Most of the gauge readings were at the level of 10^{-11} mbar except for that near the internal target area, which was $\approx 4 \times 10^{-10}$ mbar. The measured effective vacuum experienced by the stored ions was in agreement with the vacuum gauge readings.

With a derived effective vacuum of 2×10^{-10} mbar, the theoretical beam loss rate owing to ion gas collisions [58] was calculated to be 3×10^{-4} min^{-1}, corresponding to a storage lifetime of approximately 3333 min. This value was more than two times higher than the measured storage lifetime of 1359(107) min when electron cooling was OFF (see Table 1). Theoretical calculations of the ion storage lifetimes involve a wide range of parameters for collisions between the ion beam and residual gas inside a vacuum pipe [58]. These parameters change over time. The parameters used in the theoretical calculations, such as the temperature and gas composition inside the vacuum pipe, may differ from the actual parameters of the CSRe ring during experiments [60]. However, the experimental results were consistent in magnitude with the theoretical estimates. This confirms the

reliability of our methodology and indicates that the vacuum levels inferred from the ion frequency drifts accurately reflect the actual vacuum conditions within the storage ring.

5 Summary and outlook

In this study, we developed a novel method to calibrate the AFC curve of the Schottky detection system at the CSRe storage ring. Following calibration, a significant improvement in the accuracy of the peak position and peak area determination was observed in the revolution frequency spectra of the many ions stored in the ring. Using the AFC-normalized Schottky frequency spectra, the storage lifetimes (decay constants) of the $^{56}Fe^{26+}$ ions were determined with high precision at 13.7 and 116.4 MeV/u, despite frequency shifts or frequency spreading increases during the experiment. The experimental decay constants of the ions stored in the ring aligned with the theoretical calculations. Additionally, when electron cooling was switched off, the effective vacuum experienced by the stored ions was deduced from the frequency drift rate. The results showed that the vacuum was of the order of 10^{-10} mbar, which is consistent with the order of magnitude displayed by the vacuum gauge. The vacuum condition is one of the key parameters that limits the storage lifetime of highly charged ions in the storage ring. Our findings suggest that stronger vacuum pumps are required at the internal target position of the CSRe if a longer beam lifetime is required.

This method serves as a useful tool in storage ring Schottky frequency spectrum mass spectrometry to obtain accurate ion lifetimes. When electron cooling is enabled, this method can mitigate the negative effects of the irregularities caused by electron cooling device instabilities. When the electron cooling is turned off, collisions with the residual gas cause the ions to lose energy. This results in a broadening of the ion revolution frequency and shift in the frequency center. Accurate and reliable lifetime results were obtained using the method developed in this study. Thus, the method improved precision, increased the capability of beam lifetime measurements with many ions in the ring, and complemented the single-ion decay-measurement method. This new method extends the lifetime measurement method to uncooled beams. The validity and usefulness of this method were demonstrated in this study by the precise storage lifetime measurement of a stable $^{56}Fe^{26+}$ ion beam. The method developed at the CSRe can easily be adapted to other running storage ring facilities, such as the ESR at GSI in Darmstadt, Germany [9] and the R3-Ring at RIKEN in Saitama, Japan [11, 62].

One focus of next-generation Schottky mass spectrometry is the simultaneous measurement of the masses and lifetimes of short-lived ions [40]. Disabling electron cooling can extend the applicability of the technique from the minute range to the tens-of-milliseconds range for the fast broadband detection of exotic nuclei. Moreover, new Schottky detectors with higher particle sensitivities and transverse position measurement capability have been built for next-generation storage rings [16]. In this context, the amplitude normalization of the frequency spectra using the AFCs of the Schottky detector system can play a significant role in precise mass and life measurements using many ions. The methodology developed in this study will serve as a foundational component for the advancement of Schottky mass spectrometry, for example, at SRing [22, 63], which is anticipated to be pivotal for the discovery and precise measurement of exotic nuclei in future endeavors [64].

Acknowledgements We would like to extend our gratitude to Prof. F. Caspers for his insightful comments on the measurement principles, which greatly improved our manuscript. Suggestions for the vacuum calculations from Dr. Yingli Xue and Dr. Cheng Luo are gratefully acknowledged.

Author contributions All authors contributed to the study conception and design. Material preparation, data collection and analysis were performed by Qian Wang, Xin-Liang Yan, Hong-Yang Jiao, Yin-Fang Luo, Zu-Yi Chen, and Yue Yu. The first draft of the manuscript was written by Qian Wang and Xin-Liang Yan, and all authors commented on previous versions of the manuscript. All authors read and approved the final manuscript.

Data availability The data that support the findings of this study are openly available in Science Data Bank at https://cstr.cn/31253.11.sciencedb.j00186.00393 and https://www.doi.org/10.57760/sciencedb.j00186.00393.

Declarations

Conflict of interest The authors declare that they have no conflict of interest.

References

1. F.G. Kondev, M. Wang, W.J. Huang et al., The NUBASE2020 evaluation of nuclear physics properties. Chin. Phys. C. **45**, 03001 (2021). https://doi.org/10.1088/1674-1137/abddae
2. X.W. Xia, Y. Lim, P.W. Zhao et al., The limits of the nuclear landscape explored by the relativistic continuum Hartree–Bogoliubov theory. Atom. Data Nucl. Data **121–122**, 1–215 (2018). https://doi.org/10.1016/j.adt.2017.09.001
3. L. Neufcourt, Y.C. Cao, S.A. Giuliani et al., Quantified limits of the nuclear landscape. Phys. Rev. C **101**, 044307 (2020). https://doi.org/10.1103/PhysRevC.101.044307
4. Y.H. Zhang, Yu.A. Litvinov, U. Uesaka et al., Storage ring mass spectrometry of nuclear structure and astrophysics research. Phys. Scr. **91**, 073002 (2016). https://doi.org/10.1088/0031-8949/91/7/073002
5. G.X. Dai, Schottky mass spectroscope. Nucl. Phys. Rev. **14**, 239–242 (1997). https://doi.org/10.11804/NuclPhysRev.14.04.239

6. Yu.A. Litvinov, F. Bosch, Beta decay of highly charged ions. Rep. Prog. Phys. **74**, 016301 (2011). https://doi.org/10.1088/0034-4885/74/1/016301
7. Yu.A. Litvinov, S. Bishop, K. Blaum et al., Nuclear physics experiments with ion storage rings. Nucl. Instr. Methods Phys. Res. B. **317**, 603–616 (2013). https://doi.org/10.1016/j.nimb.2013.07.025
8. T. Faestermann, Lifetime measurements of nuclei in few-electron ions. Phys. Scr. **2015**, 014003 (2015). https://doi.org/10.1088/0031-8949/2015/T166/014003
9. B. Franzke, The heavy ion storage and cooler ring project ESR at GSI. Nucl. Inst. Methods Phys. Res. B. **24–25**, 18–25 (1987). https://doi.org/10.1016/0168-583X(87)90583-0
10. J.W. Xia, W.L. Zhan, B.W. Wei et al., The heavy ion cooler-storage-ring project (HIRFL-CSR) at Lanzhou. Nucl. Inst. Methods Phys. Res. A. **488**, 11–25 (2002). https://doi.org/10.1016/S0168-9002(02)00475-8
11. A. Ozawa, T. Uesaka, M. Wakasugi, The rare-RI ring. Prog. Theor. Exp. Phys. **2012**, 03C0009 (2012). https://doi.org/10.1093/ptep/pts060
12. J. Zhou, Y.J. Yuan, J.C. Yang et al., Study of nuclear mass measurement by electron cooling mode in CSRe. Nucl. Phys. Rev. **26**, 33–36 (2009). https://doi.org/10.11804/NuclPhysRev.26.01.033
13. F. Bosch, Y.A. Litvinov, T. Stöhlker, Nuclear physics with unstable ions at storage rings. Prog. Part. Nucl. Phys. **73**, 84–140 (2013). https://doi.org/10.1016/j.ppnp.2013.07.002
14. F. Suzaki, Y. Abe, A. Ozawa et al., A resonant Schottky pick-up for Rare-RI Ring at RIKEN. Phys. Scr. **2015**, 014059 (2015). https://doi.org/10.1088/0031-8949/2015/T166/014059
15. B. Wu, J.C. Yang, J.W. Xia et al., The design of the Spectrometer Ring at the HIAF. Nucl. Inst. Methods Phys. Res. A **881**, 27–35 (2018). https://doi.org/10.1016/j.nima.2017.08.017
16. M. Hansli, A. Penirschke, R. Jakoby et al., Current status of the Schottky sensor system at the CR at FAIR, in *Proceedings of IBIC2013*. 2nd International Beam Instrumentation Conference, Oxford, UK, pp. 907–909 (2013). https://accelconf.web.cern.ch/ibic2013/papers/wepf35.pdf
17. J.W. Xia, W.L. Zhan, B.W. Wei et al., HIRFL-CSR complex. Chin. Phys. C. **33**, 804–810 (2009). https://doi.org/10.1088/1674-1137/33/9/019
18. M. Wang, H.S. Xu, J.W. Xia et al., First isochronous mass measurements at CSRe. Int. J. Mod. Phys. E. **18**, 352–358 (2009). https://doi.org/10.1142/S0218301309012380
19. X. Zhou, M. Wang, Y.H. Zhang et al., $B\rho$-defined Isochronous mass spectrometry at the storage ring CSRe. Nucl. Sci. Tech. **35**, 213 (2024). https://doi.org/10.1007/s41365-024-01587-y
20. Q. Zeng, M. Wang, X.H. Zhou et al., Half-life measurement of short-lived $^{94m}Ru^{44+}$ using isochronous mass spectrometry. Phys. Rev. C (2017). https://doi.org/10.1103/PhysRevC.96.031303
21. Y.D. Zang, R.S. Mao, J.X. Wu et al., Schottky beam diagnostic system at CSRe. High Power Laser Part. Beams **23**, 1899–1903 (2011). https://doi.org/10.3788/HPLPB20112307.1899
22. J.X. Wu, Y.D. Zang, F. Nolden et al., Performance of the resonant Schottky pickup at CSRe. Nucl. Inst. Methods Phys. Res. B **317**, 623–628 (2013). https://doi.org/10.1016/j.nimb.2013.08.017
23. F. Nolden, P. Hülsmann, Yu.A. Litvinov et al., A fast and sensitive resonant Schottky pick-up for heavy ion storage rings. Nucl. Inst. Methods Phys. Res. A **659**, 69–77 (2011). https://doi.org/10.1016/j.nima.2011.06.058
24. L.X. Chen, G.Q. Xiao, Z.Y. Guo et al., Study of design and test of Schottky pick up. Nucl. Phys. Rev. **21**, 30–33 (2004). https://doi.org/10.11804/NuclPhysRev.21.01.030
25. X.L. Tu, X.C. Chen, J.T. Zhang et al., First application of combined isochronous and Schottky mass spectrometry: Half-lives of fully ionized $^{49}Cr^{24+}$ and $^{53}Fe^{26+}$ atoms. Phys. Rev. C **97**, 014321 (2018). https://doi.org/10.1103/PhysRevC.97.014321
26. Q. Wang, X.C. Chen, M. Wang et al., Remote control system of data acquisition for the Schottky resonator at CSRe. Nucl. Phys. Rev. **38**, 430–437 (2021). https://doi.org/10.11804/NuclPhysRev.38.2021018
27. Q. Wang, X.L. Yan, X.C. Chen et al., Spectral baseline estimation using penalized least squares with weights derived from the Bayesian method. Nucl. Sci. Tech. **33**, 148 (2022). https://doi.org/10.1007/s41365-022-01132-9
28. Y. Li, X. Wang, H. Zhang et al., Implementation of a dipole magnet power supply control system to improve magnetic field stability at the CSRe storage ring facility for precision mass measurement. Nucl. Inst. Methods Phys. Res. A **1049**, 168108 (2023). https://doi.org/10.1016/j.nima.2023.168108
29. J. Borer, P. Bramham, H.G. Hereward et al., Non-destructive diagnostics of coasting beams with schottky noise, in *Proceedings of 9th International Conference on High-energy Accelerators*, Stanford, USA, pp. 53–56 (1974). https://cds.cern.ch/record/310532
30. X.L. Tu, M. Wang, Yu.A. Litvinov et al., Precision isochronous mass measurements at the storage ring CSRe in Lanzhou. Nucl. Inst. Methods Phys. Res. A. **654**, 213–218 (2011). https://doi.org/10.1016/j.nima.2011.07.018
31. X. Zhou, M. Wang, Y.J. Yuan et al., Charge resolution in the isochronous mass spectrometry and the mass of ^{51}Co. Nucl. Sci. Tech. **32**, 37 (2021). https://doi.org/10.1007/s41365-021-00876-0
32. X. Zhou, M. Wang, Y.H. Zhang et al., Mass measurements show slowdown of rapid proton capture process at waiting-point nucleus ^{64}Ge. Nat. Phys. **19**, 1091–1097 (2022). https://doi.org/10.1038/s41567-023-02034-2
33. M. Wang, Y.H. Zhang, X. Zhou et al., Mass measurement of upper *fp*-Shell $N = Z - 2$ and $N = Z - 1$ nuclei and the importance of three-nucleon force along the $N = Z$ line. Phys. Rev. Lett. **130**, 192501 (2023). https://doi.org/10.1103/PhysRevLett.130.192501
34. B. Franzke, H. Geissel, G. Münzenberg, Mass and lifetime measurements of exotic nuclei in storage rings. Mass Spectrom. Rev. **27**(5), 428–469 (2008). https://doi.org/10.1002/mas.20173
35. K. Beckert, S. Cocher, B. Franzke et al., The ESR schottky-dagnosis-system, in *Proceedings of 2nd European Particle and Accelerator Conference. 2nd European Particle and Accelerator Conference*, Nice, France, pp. 777–779 (1990). https://accelconf.web.cern.ch/e90/PDF/EPAC1990_0777.PDF
36. Z. Du, P.L. He, G.Y. Zhu et al., Development of a diagonal-cut type beam position monitor for the booster ring in the high intensity heavy-ion accelerator facility project. Rev. Sci. Instrum. **93**, 043306 (2022). https://doi.org/10.1063/5.0083344
37. M. Bregman, M. Calvetti, G. Carron et al., Measurement of antiproton lifetime using the ice storage ring. Phys. Lett. B **78**, 174–175 (1978). https://doi.org/10.1016/0370-2693(78)90376-3
38. M.S. Sanjari, D. Dmytriiev, Yu.A. Litvinov et al., A 410 MHz resonant cavity pickup for heavy ion storage rings. Rev. Sci. Instrum. **91**, 083302 (2020). https://doi.org/10.1063/5.0009094
39. P. Kienle, F. Bosch, P. Bühler et al., High-resolution measurement of the time-modulated orbital electron capture and of the β^+ decay of hydrogen-like $^{142}Pm^{60+}$ ions. Phys. Lett. B **726**(4–5), 638–645 (2013). https://doi.org/10.1016/j.physletb.2013.09.033
40. Yu.A. Litvinov, R.J. Chen, Radioactive decays of stored highly charged ions. Eur. Phys. J. A **59**(5), 102 (2023). https://doi.org/10.1140/epja/s10050-023-00978-w
41. M. Steck, K. Beckert, H. Eickhoff et al., Anomalous temperature reduction of electron-cooled heavy ion beams in the storage ring ESR. Phys. Rev. Lett. **77**, 3803–3806 (1996). https://doi.org/10.1103/PhysRevLett.77.3803
42. M. Steck, G. Bisoffi, M. Blum et al., Electron cooling of heavy ions. Nucl. Inst. Methods Phys. Res. A **287**, 324–327 (1990). https://doi.org/10.1016/0168-9002(90)91817-U

43. M. Steck, P. Beller, K. Beckert et al., Electron cooling experiments at the ESR. Nucl. Inst. Methods Phys. Res. A **532**, 357–365 (2004). https://doi.org/10.1016/j.nima.2004.06.065
44. M. Steck, Yu.A. Litvinov, Heavy-ion storage rings and their use in precision experiments with highly charged ions. Prog. Part. Nucl. Phys. **115**, 103811 (2020). https://doi.org/10.1016/j.ppnp.2020.103811
45. J. Eichler, T. Stoehlker, Radiative electron capture in relativistic ion-atom collisions and the photoelectric effect in hydrogen-like high-Z systems. Phys. Rep. **439**, 1–99 (2007). https://doi.org/10.1016/j.physrep.2006.11.003
46. D. Boussard, Schottky noise and beam transfer function diagnostics, in *CAS - CERN Accelerator School: 5th advanced accelerator physics course*. CAS - CERN Accelerator School: 5th advanced accelerator physics course, Rhodes, Greece, pp. 749–782 (1995). https://doi.org/10.5170/CERN-1995-006.749
47. D.Y. Chen, H.B. Wang, W.Q. Wen et al., Longitudinal Schottky signal spectrum at heavy-ion storage ring: simulation and analysis. Sci. Sin.-Phys. Mech. Astron. **50**(1), 013002 (2024). https://doi.org/10.1360/SSPMA-2024-0038. (**in Chinese**)
48. G.Y. Qiu, *Circuit*, 5th edn. (Higher Education Press, Beijing, 2006) (in Chinese)
49. X.X. Yang, Z.X. Yi, *Fundamentals of Microwave Technology*, 3rd edn. (Tsinghua University Press, Beijing, 2021) (in Chinese)
50. P.B. Wilson, Introduction to wakefields and wake potentials. AIP Conf. Proc. **184**, 525–569 (1989). https://doi.org/10.1063/1.38045
51. X. Yang, J. Li, L. Mao et al., Electron cooling experiments in CSR. Sci. Sin.-Phys. Mech. Astron. **54**, 274–278 (2011). https://doi.org/10.1007/s11433-011-4503-x
52. L.J. Mao, H. Zhao, X.D. Yang et al., Longitudinal Electron cooling experiments at HIRFL-CSRe. Nucl. Inst. Methods Phys. Res. A **808**, 29–34 (2016). https://doi.org/10.1016/j.nima.2015.10.095
53. I.S. Dmitriev, V.P. Zaikov, E.A. Kral'kina et al., On the target thickness to attain equilibrium charge distribution in a beam of fast ions. Nucl. Inst. Methods Phys. Res. B. **14**, 515–526 (1986). https://doi.org/10.1016/0168-583X(86)90148-5
54. B. Franzke, Interaction of stored ion beams with the residual gas, in *CAS - CERN Accelerator School: 4th advanced accelerator physics course*. CAS - CERN Accelerator School: 4th advanced accelerator physics course, Dourdan, France, pp. 100–119 (1992). https://doi.org/10.5170/CERN-1992-001.100
55. H. Poth, Electron cooling: Theory, experiment, application. Phys. Rep. **196**(3–4), 135–297 (1990). https://doi.org/10.1016/0370-1573(90)90040-9
56. I.Y. Tolstikhina, V.P. Shevelko, Collision processes involving heavy many-electron ions interacting with neutral atoms. Phys.-Uspekhi. **56**(3), 213–242 (2013). https://doi.org/10.3367/UFNe.0183.201303a.0225
57. X.Y. Zhang, Master Thesis, University of Chinese Academy of Sciences (2005) (in Chinese)
58. Y.L. Xue, X.H. Cai, D.Y. Yu et al., Loss mechanism and lifetime of ion beam in HIRFL-CSRe. Nucl. Phys. Rev. **25**, 355–361 (2008). https://doi.org/10.1088/1742-6596/163/1/012075
59. A.S. Schlacher, J.W. Stearns, W.G. Graham et al., Electron capture for fast highly charged ions in gas targets: an empirical scaling rule. Phys. Rev. A **27**, 3372(R) (1983). https://doi.org/10.1103/PhysRevA.27.3372
60. H.B. Wang, Phd. Thesis, University of Chinese Academy of Sciences (2017) (in Chinese)
61. O.B. Tarasov, D. Bazin, LISE++: Radioactive beam production with in-flight separators. Nucl. Inst. Methods Phys. Res. B. **266**, 4657–4664 (2008). https://doi.org/10.1016/j.nimb.2008.05.110
62. D. Dmytriiev, M.S. Sanjari, Yu.A. Litvinov et al., Position sensitive resonant Schottky cavities for heavy ion storage rings. Nucl. Inst. Methods Phys. Res. B **463**, 320–323 (2020). https://doi.org/10.1016/j.nimb.2019.04.074
63. J.C. Yang, J.W. Xia, G.Q. Xiao et al., High intensity heavy ion accelerator facility (HIAF) in China. Nucl. Inst. Methods Phys. Res. B **317**, 263–265 (2013). https://doi.org/10.1016/j.nimb.2013.08.046
64. T. Yamaguchi, H. Koura, Yu.A. Litvinov et al., Masses of exotic nuclei. Prog. Part. Nucl. Phys. **120**, 103882 (2021). https://doi.org/10.1016/j.ppnp.2021.103882

Authors and Affiliations

Qian Wang[1] · Xin-Liang Yan[1,2] · Guang-Yu Zhu[1] · Shahab Sanjari[3,4] · Li-Jun Mao[1,2] · He Zhao[1,2] · Yuri A. Litvinov[3] · Rui-Jiu Chen[3] · Meng Wang[1,2] · Yu-Hu Zhang[1,2] · You-Jin Yuan[1,2] · Jun-Xia Wu[1,2] · Hong-Yang Jiao[1,2] · Yue Yu[1,2] · Zu-Yi Chen[1,2] · Yin-Fang Luo[1,2]

✉ Qian Wang
wangqian2016@impcas.ac.cn

✉ Xin-Liang Yan
yanxinliang08@impcas.ac.cn

✉ Meng Wang
wangm@impcas.ac.cn

[1] Institute of Modern Physics, Chinese Academy of Sciences, Lanzhou 730000, China

[2] University of Chinese Academy of Sciences, Beijing 100049, China

[3] GSI Helmholtzzentrum für Schwerionenforschung, Planckstrasse 1, 64291 Darmstadt, Germany

[4] FH Aachen University of Applied Sciences, Heinrich-Mussmann-Str. 1, 52428 Jülich, Germany